BJP British Journal of Pharmacology

DOI:10.1111/bph.12686
www.brjpharmacol.org

RESEARCH PAPER

Effects of arginine 10 to lysine substitution on ω-conotoxin CVIE and CVIF block of $Ca_v2.2$ channels

G Berecki[1], N L Daly[2,3], Y H Huang[2], S Vink[2], D J Craik[2], P F Alewood[2] and D J Adams[1]

[1]*Health Innovations Research Institute, RMIT University, Melbourne, Vic, Australia,* [2]*Division of Chemistry and Structural Biology, Institute for Molecular Bioscience, The University of Queensland, Brisbane, Qld, Australia, and* [3]*Centre for Biodiscovery and Molecular Development of Therapeutics, School of Pharmacy and Molecular Sciences, James Cook University, Cairns, Qld, Australia*

Correspondence
Géza Berecki, Health Innovations Research Institute, RMIT University, PO Box 71, Bundoora, Victoria 3083, Australia. E-mail: geza.berecki@rmit.edu.au

Keywords
N-type VGCC; $Ca_v2.2$ channel; ω-conotoxin; holding potential; NMR; serum stability

Received
5 November 2013
Revised
28 February 2014
Accepted
5 March 2014

BACKGROUND AND PURPOSE

ω-Conotoxins CVIE and CVIF (CVIE&F) selectively inhibit $Ca_v2.2$ channels and are lead molecules in the development of novel analgesics. At physiological membrane potentials, CVIE&F block of $Ca_v2.2$ channels is weakly reversible. To improve reversibility, we designed and synthesized arginine CVIE&F analogues in which arginine was substituted for lysine at position 10 ([R10K]CVIE&F), and investigated their serum stability and pharmacological actions on voltage-gated calcium channels (VGCCs).

EXPERIMENTAL APPROACH

Changes in peptide structure due to R10K substitution were assessed by NMR. Peptide stability in human serum was analysed by reversed-phase HPLC and MS over a 24 h period. Two-electrode voltage-clamp and whole-cell patch clamp techniques were used to study [R10K]CVIE&F effects on VGCC currents in *Xenopus* oocytes and rat dorsal root ganglion neurons respectively.

KEY RESULTS

R10K substitution did not change the conserved ω-conotoxin backbone conformations of CVIE&F nor the ω-conotoxin selectivity for recombinant or native $Ca_v2.2$ channels, although the inhibitory potency of [R10K]CVIF was better than that of CVIF. At −80 mV, the R10K chemical modification significantly affected ω-conotoxin–channel interaction, resulting in faster onset kinetics than those of CVIE&F. Heterologous and native $Ca_v2.2$ channels recovered better from [R10K]CVIE&F block than CVIE&F. In human serum, the ω-conotoxin half-lives were 6–10 h. CVIE&F and [R10K]CVIE&F were more stable than CVID.

CONCLUSIONS AND IMPLICATIONS

R10K substitution in CVIE&F significantly alters the kinetics of ω-conotoxin action and improves reversibility without diminishing conotoxin potency and specificity for the $Ca_v2.2$ channel and without diminishing the serum stability. These results may help generate ω-conotoxins with optimized kinetic profiles for target binding.

Abbreviations

N-type VGCC, neuronal-type voltage-gated calcium channel; DRG, dorsal root ganglion; CVID, ω-conotoxin CVID; CVIE, ω-conotoxin CVIE; CVIF, ω-conotoxin CVIF; MVIIA, ω-conotoxin MVIIA; HP, holding potential; RP-HPLC, reversed-phase HPLC; Vc1.1, α-conotoxin Vc1.1

Introduction

Neuronal (N)-type ($Ca_v2.2$) voltage-gated calcium channels (VGCCs; see Alexander *et al.*, 2013) are prominently involved in nociception, and their inhibition can cause analgesia in animals and humans (Altier and Zamponi, 2004; Snutch, 2005; McGivern, 2006; Zamponi *et al.*, 2009). Several ω-conotoxins selectively inhibit N-type VGCCs, so are considered attractive molecules to use in drug design (Olivera *et al.*, 1994; Adams *et al.*, 2012; Lewis *et al.*, 2012). ω-Conotoxins (also called 'ω-conopeptides') are small disulfide-rich peptides isolated from the venom of marine cone snails. Conopeptide biochemistry, synthesis, structure–activity relationships and pharmacology have been comprehensively studied. A number of essential ω-conotoxin residues that interact with VGCCs have been identified and the pharmacophore of different ω-conotoxins can exhibit considerable differences (Terlau and Olivera, 2004; Bulaj and Olivera, 2008; Bingham *et al.*, 2010; Adams *et al.*, 2012; Lewis *et al.*, 2012; Vink and Alewood, 2012).

Intrathecal administration of ω-conotoxins can cause marked antinociception in rodent models of acute, chronic, inflammatory and neuropathic pain (Schroeder *et al.*, 2006). Therefore, these conopeptides have potential as lead structures for novel analgesics (McGivern, 2006). However, their use in pain management is limited because of their poor absorption, poor stability (Craik and Adams, 2007) and frequently reported adverse actions and side effects in clinical trials (Schmidtko *et al.*, 2010). Although case studies provide support for the use of ω-conotoxin MVIIA (ziconotide) in combination with morphine, baclofen or hydromorphone (Jaggi *et al.*, 2011), strong evidence-based data are limited (Wallace *et al.*, 2010). Better tolerated, improved and/or new N-type VGCC inhibitors are needed to help form the next generation of drugs to treat chronic pain.

Recently, we identified ω-conopeptides CVIE and CVIF (CVIE&F) as potent and selective N-type VGCC blockers and nociceptive signalling inhibitors because they both reversed allodynia in a rat partial nerve ligation model (Berecki *et al.*, 2010). In the *Xenopus* oocyte heterologous expression system, $Ca_v2.2$ (α_{1B}) calcium channels, co-expressed with $\alpha_2\delta_1$ and β_3 (inactivating-type) subunits, showed weak recovery from CVIE or CVIF block at a close-to-physiological (–80 mV) membrane holding potential (HP). However, recovery was reversible at –125 mV (Berecki *et al.*, 2010). This suggested that CVIE&F have higher affinity for inactivated channels, a biophysical property also known for ω-conopeptides GVIA, MVIIA and SNX-331, an MVIIC derivative (Stocker *et al.*, 1997). Remarkably, co-expression of the non-inactivating (or slowly inactivating) type β_{2a} subunit with $Ca_v2.2$ (α_{1B}) and $\alpha_2\delta_1$ also led to complete channel recovery from CVIE or CVIF block at –80 mV. These findings directly linked VGCC inactivation and ω-conotoxin block reversibility (Berecki *et al.*, 2010).

Single residues on the ω-conopeptide molecule can have a significant impact on binding and/or dissociation from binding site(s) close to the $Ca_v2.2$ (α_{1B}) channel pore. Loop 2 of ω-conotoxins is the primary structural motif involved in binding to the $Ca_v2.2$ channel (Kim *et al.*, 1994). In loop 2, the amino acid in position 10 (hydroxyproline, arginine and lysine in ω-conotoxins GVIA, MVIIA and CVID, respectively) has been shown to affect $Ca_v2.2$ channel inhibition (Adams *et al.*, 2003) and reversibility (Mould *et al.*, 2004). For example, the K10R-substituted CVID ([K10R]CVID) inhibits neurotransmitter release significantly less than CVID in preganglionic cholinergic nerve terminals (Adams *et al.*, 2003). In *Xenopus* oocytes, [K10R]CVID impairs reversibility of $Ca_v2.2$ channel inhibition, whereas the R10K mutation in MVIIA increases the reversibility of this process (Mould *et al.*, 2004). CVID inhibition of heterologously expressed $Ca_v2.2$ channels is also more reversible than that of MVIIA (Mould *et al.*, 2004).

In this study, we investigated how the 10th amino acid influences ω-conotoxin CVIE&F efficacy at the $Ca_v2.2$ channel. We substituted arginine for lysine at position 10 to create [R10K]CVIE and [R10K]CVIF. We analysed the serum stability of CVIE&F and [R10K]CVIE&F, and determined the effect of R10K substitution on ω-conotoxin backbone conformation. In a series of electrophysiological experiments, we studied the potency, selectivity, voltage dependence and kinetics of conotoxin–VGCC interaction, and the reversibility of ω-conotoxin action on recombinant and native $Ca_v2.2$ channels in *Xenopus* oocytes and dorsal root ganglion (DRG) neurons respectively.

Methods

Conopeptide synthesis, quantitation, MS and HPLC analysis

CVIE&F and [R10K]CVIE&F were synthesized as previously described (Berecki *et al.*, 2010). Briefly, peptides were manually synthesized using Boc *in situ* neutralization solid-phase peptide synthesis (Schnölzer *et al.*, 1992). They were then purified and quantified using reversed-phase HPLC (RP-HPLC) with an external reference standard.

^{1}H NMR analysis

R10K analogues were dissolved in 90% H_2O : 10% D_2O to give a final concentration of 1 mM (pH 4). Spectra were recorded on a 600 MHz AVANCE NMR spectrometer (Bruker, Bremen, Germany) and included a high-resolution 1D NMR spectrum and homonuclear two-dimensional TOCSY, NOESY and DQF-COSY spectra. All spectra were recorded at 290 K with an inter-scan delay of 1 s. TOCSY and NOESY spectra were acquired with mixing times of 80 and 200 ms respectively. Standard Bruker pulse sequences were used with a WATERGATE pulse sequence for solvent suppression. NMR data were processed using XEASY.

Functional expression of VGCCs in Xenopus oocytes

All animal experiments were performed in accordance with the guidelines of the *National Health and Medical Research Council (NHMRC) Code of Practice for the Care and Use of Animals in Research in Australia* and approved by the University of Queensland and RMIT University animal ethics committees. Stage V–VI oocytes from *Xenopus laevis* were surgically removed and cultured as previously described (Berecki *et al.*, 2010). Capped cRNA transcripts encoding VGCC pore-forming and auxiliary subunits of rat $Ca_v2.2$ $\alpha_{1B\text{-}b}$

(N-type, peripheral isoform), rat $Ca_v1.3$ α_{1D} (L-type) and rat β_3 (provided by Dr D Lipscombe, Brown University, Providence, RI, USA); rabbit $Ca_v1.2$ α_{1C} (L-type) and rat β_{2a} (provided by Dr G Zamponi, University of Calgary, Calgary, Canada); and rabbit $\alpha_2\delta_1$ (provided by Drs F Hofmann and N Klugbauer, Technische Universität München, Munich, Germany) were synthesized using the mMessage mMachine *in vitro* transcription kit (Ambion, Life Technologies Australia Pty Ltd, Mulgrave, Vic, Australia). Each oocyte was injected with 50 nL of solution containing a mixture of cRNAs encoding an $\alpha_{1B\text{-}b}$, α_{1C} or α_{1D} pore-forming subunit (5 ng); $\alpha_2\delta_1$ (5 ng); and a β_3 (5 ng) or β_{2a} (0.5 ng) auxiliary subunit. All studies involving animals are reported in accordance with the ARRIVE guidelines for reporting experiments involving animals (Kilkenny *et al.*, 2010; McGrath *et al.*, 2010).

For experiments with rat $Ca_v2.3$ (α_{1E}; R-type) and rabbit $Ca_v2.1$ (α_{1A}; P/Q-type) (both provided by Dr G Zamponi), the oocyte nucleus was first injected with 9 nL of $Ca_v2.1$ (α_{1A}) cDNA (4.5 ng per cell) or $Ca_v2.3$ (α_{1E}) cDNA (4.5 ng per cell) subunits. The oocyte cytoplasm was then injected with auxiliary subunit cRNAs as described earlier. After injection, oocytes were kept at 18°C for 3–7 days for recombinant calcium channel expression, as previously described (Berecki *et al.*, 2010).

Xenopus *oocyte electrophysiology*

Depolarization-activated Ba^{2+} currents (I_{Ba}) were recorded using a two-electrode virtual ground voltage-clamp circuit with a GeneClamp 500B amplifier controlled by a Digi-Data1332 acquisition system and Clampex9.2 software (Molecular Devices, Sunnyvale, CA, USA). Before the recording, oocytes were injected with 30 nL of 50 mM BAPTA to eliminate endogenous Ca^{2+}-activated Cl^- conductance. During the recording, oocytes were placed in a 0.1 mL recording chamber and superfused at a constant rate of ~3 mL min^{-1}. The external bath solution contained (in mM) 5 $BaCl_2$, 85 tetraethylammonium hydroxide (TEA-OH), 5 KCl and 10 HEPES (pH 7.4) (adjusted with methanesulfonic acid).

Borosilicate glass microelectrodes were filled with 3 M KCl and had resistances of 0.4–1.2 MΩ. Oocytes were voltage-clamped at various HPs, and membrane currents were elicited by 200 ms step depolarizations to 0 mV ($Ca_v2.2$ and $Ca_v1.2$), +10 mV ($Ca_v2.1$), +10 mV ($Ca_v2.3$) or –20 mV ($Ca_v1.3$), applied every 10 s. Leak and capacitive currents were subtracted using a –P/4 pulse protocol. Current amplitudes were monitored online using the Clampex 9.2 software package. Membrane currents were filtered at 1 or 2 kHz, digitized at 5 kHz and stored on a computer hard drive.

DRG neurons and patch-clamp recordings

Experiments followed the *NHMRC Code of Practice for the Care and Use of Animals in Research in Australia* guidelines and were approved by the University of Queensland and RMIT University animal ethics committees. DRG neurons were enzymatically dissociated from the ganglia of 4- to 14-day-old, Wistar rats of either sex, as described previously (Motin *et al.*, 2007). Cells were plated on poly-D-lysine/laminin-coated 12 mm round coverslips (BD Biosciences Discovery Labware, Bedford, MA, USA) and were cultured at 37°C in 5% CO_2 in DMEM (Invitrogen Life Technologies) supplemented with 10% (v v^{-1}) FBS (Invitrogen), 50 IU·mL^{-1} penicillin and 50 μg·mL^{-1} streptomycin (Invitrogen). DRG neurons, used for patch-clamp experiments within 24–48 h of isolation, were constantly perfused with a solution containing (in mM) 150 tetraethylammonium chloride, 2 $BaCl_2$, 10 D-glucose and 10 HEPES–NaOH (pH 7.4).

Borosilicate glass electrodes were filled with an internal solution containing (in mM) 140 CsCl, 1 $MgCl_2$, 5 MgATP, 0.1 Na-GTP, 5 BAPTA-Cs_4 and 10 HEPES–CsOH (pH 7.3) and had resistances of 1.5–2.5 MΩ. Patch-clamp recordings were performed with a Multiclamp 700B amplifier (Molecular Devices) at room temperature (21–23°C). Under voltage-clamp conditions, whole-cell I_{Ba} were elicited by 200 ms step depolarizations to 0 mV, from a HP of –80 mV, applied every 15 s. Currents were filtered at 2 kHz and sampled at 5 kHz. Leak and capacitative currents were subtracted using a –P/4 pulse protocol. Data were stored digitally on a computer for further analysis.

Serum stability assay

ω-Conotoxin stability was assessed using a method modified from a previous study (Clark *et al.*, 2010). In brief, CVID, CVIE&F, [R10K]CVIE&F and α-conotoxin Vc1.1 (Vc1.1) were incubated in human serum (Sigma-Aldrich, Castle Hill, NSW, Australia) individually at a concentration of 20 μM for 0, 1, 2, 3, 4, 6, 8, 12 and 24 h at 37°C. Triplicate aliquots of each peptide in serum were sampled at the stipulated times and the serum proteins were denatured by incubating with 40 μL of 6 M urea for 10 min at 4°C. Samples were then treated with 40 μL of 20% trichloroacetic acid for 10 min at 4°C. Precipitated serum proteins were then spun down at 17 000× *g*. Supernatants of each sample were analysed by RP-HPLC on an analytical column using a linear 1% min^{-1} gradient of solvent B (0.045% TFA in 90% acetonitrile) at a flow rate of 0.3 mL·min^{-1}. The amount of intact peptide remaining at a given time point was quantified by comparing the height of the peptide peak at 215 nm with that of the original peak at time zero.

Three sets of control experiments were included: the

(1) comparison of the stability of reduced Vc1.1 and CVIE&F with native peptides;
(2) measurement of the stability of Vc1.1 and CVIE at 4°C at 0, 3 and 6 h time points; and
(3) preparation of PBS-treated peptides at 0 and 24 h time points and evaluation of peptide loss due to sample handling or serum protein binding (around 5%).

Peptide reduction was achieved by incubating peptides with 100 mM DTT at 60°C for 30 min and then alkylating them with 25 mM iodoacetamide for 15 min at room temperature.

Chemicals and drugs

All chemical reagents were obtained from Sigma-Aldrich. ω-Conotoxins CVID, CVIE&F and MVIIA were prepared as previously described (Nielsen *et al.*, 1999; Lewis *et al.*, 2000), diluted to the final concentration immediately before the experiment and bath applied. Drug/molecular target

nomenclature conforms to the *British Journal of Pharmacology's Concise Guide to Pharmacology* (Alexander *et al.*, 2013).

Curve fitting and statistical analysis

Data analysis was performed in Clampfit 9.2 (Molecular Devices) and Origin 9.0 (Microcal Software Inc., Northampton, MA, USA). Concentration–response curves were obtained by plotting averaged relative peak current amplitude values (I/I_0) versus toxin concentration, and fitting the resulting data by the Hill equation $I = I_0\{[Ctx]^{n_H}/(IC_{50}{}^{n_H} + [Ctx]^{n_H})\}$, where I_0 is the maximum peak current amplitude, [Ctx] is the concentration of ω-conotoxin, IC_{50} is the concentration that gives a half-maximal response and n_H is the Hill slope.

The percentage of I_{Ba} blocked by the toxin was determined as $(1 - I/I_0) \times 100$. The percentage of current recovered from block was defined as $[(I_{rec} - I)/(I_0 - I)] \times 100$, where I_0 is the maximum peak current amplitude and I and I_{rec} are the current amplitudes during block and after washout.

Recovery times were determined at various time points and maximum recovery was estimated when no further recovery could be observed over a 5 min period of washout. The rate of onset of toxin block was obtained by fitting the peak current amplitudes recorded during current block to a monoexponential equation $I/I_0 = A \times \exp(-t/\tau_{on})$, where A is maximal peak current amplitude, t is the time and τ_{on} is the onset time constant.

Offset time constants (τ_{off}) were obtained by fitting peak current amplitudes recorded during current recovery from block to a mono-exponential equation $I/I_0 = A[1 - \exp(-t/\tau_{off})]$, where A is maximal peak current amplitude and t is the time.

Dissociation constant (K_D) values were calculated according to $K_D = k_{off}/k_{on}$ (M), where $k_{off} = 1/\tau_{off}$ (s^{-1}) and $k_{on} = (1/\tau_{on} - k_{off})/[toxin]$ ($M^{-1}{\cdot}s^{-1}$)].

Data are mean ± SEM (n, number of experiments). Statistical analyses were performed in Sigma Plot 11.0 (Systat Software, Inc., San Jose, CA, USA) using Student's t-test for two groups or one-way ANOVA with Bonferroni's *post hoc* testing for multiple comparisons. Differences were considered statistically significant if $P < 0.05$.

Results

^{1}H NMR studies

The [R10K]CVIE&F analogue structures (Table 1) were analysed using NMR spectroscopy. Sequence-specific resonance assignments were made using TOCSY and NOESY spectra. Secondary shifts, which are sensitive to structural changes and can indicate the overall fold, were determined by subtracting random coil shifts (Wishart *et al.*, 1995) from the αH shifts. The secondary shifts of the analogues were compared with those of CVIE&F and MVIIA, as shown in Figure 1A. The similarity in shifts confirms that the overall fold is similar in all of the peptides. Therefore, the R10K analogues contain the inhibitor cystine knot motif (Craik *et al.*, 2001) present in MVIIA (Hatakeyama *et al.*, 2001; Adams *et al.*, 2003) and predicted to be present in CVIE&F (Berecki *et al.*, 2010). The three-dimensional structure of MVIIA, highlighting the cystine knot motif, is shown in Figure 1B.

Table 1

Amino acid sequence of selected ω-conotoxins

Conotoxin	Sequence and disulfide connectivity	Net charge
		
CVID	**C**KSK**G**AK**C**S*K*LM**Y**D**CC**SGS**C**SGTVGR**C***	+5
CVIE	**C**KGKGAS**C**R*R*TSYD**CC**TGS**C**R--SGR**C***	+5
[R10K]CVIE	**C**KGKGAS**C**R*K*TSYD**CC**TGS**C**R--SGR**C***	+5
CVIF	**C**KGKGAS**C**R*R*TSYD**CC**TGS**C**R--LGR**C***	+5
[R10K]CVIF	**C**KGKGAS**C**R*K*TSYD**CC**TGS**C**R--LGR**C***	+5
MVIIA	**C**KGKGAK**C**S*R*LMYD**CC**TGS**C**R--SGK**C***	+6

Conserved cysteine residues are in bold. Position 10 is in italics. Note the unchanged net charge in [R10K]CVIE&F compared with that of CVIE&F.
*C-terminal amidated.

Effect of R10K substitution on CVIE&F pharmacology

We investigated the influence of R10K substitution on CVIE&F pharmacology in *Xenopus* oocytes expressing recombinant $Ca_v2.2$ VGCCs. [R10K]CVIE&F blocked heterologously expressed $\alpha_{1B\text{-}b}/\alpha_2\delta_1/\beta_3$ and $\alpha_{1B\text{-}b}/\alpha_2\delta_1/\beta_{2a}$ VGCCs in a concentration-dependent manner (Figure 2A,B). The concentration dependence of I_{Ba} block was described by Hill equations, resulting in IC_{50} and Hill slope values shown in Table 2. IC_{50} values of the R10K analogues were similar to those reported for CVIE&F (Berecki *et al.*, 2010), except for [R10K]CVIF, which was more potent than CVIF in inhibiting $\alpha_{1B\text{-}b}/\alpha_2\delta_1/\beta_3$ VGCCs in oocytes. The Hill slope of both R10K analogues was higher than those of CVIE&F, suggesting that the interaction between the toxin and binding site on the channel changed.

We also determined [R10K]CVIE&F selectivity in the concentration range between 0.1 and 1 μM. Neither [R10K]CVIE nor [R10K]CVIF affected recombinant $Ca_v1.2$ α_{1C} (L-type) (n = 4 and 3, respectively), $Ca_v1.3$ α_{1D} (L-type) (n = 3 and 3, respectively), $Ca_v2.1$ α_{1A} (P/Q-type) (n = 6 and 6, respectively) or $Ca_v2.3$ α_{1E} (R-type) (n = 3 and 3, respectively) channels heterologously expressed in *Xenopus* oocytes (Figure 2C).

The characteristics of block and/or recovery from block by several known ω-conotoxins depend on the HP and degree of voltage-dependent inactivation of N-type VGCCs (Stocker *et al.*, 1997). Our previous results demonstrated that $Ca_v2.2$ channel recovery from CVIE or CVIF block was modulated by auxiliary β subunit isoforms, demonstrating a link between N-type VGCC inactivation and reversibility (Berecki *et al.*, 2010). In *Xenopus* oocytes, $\alpha_{1B\text{-}b}/\alpha_2\delta_1/\beta_3$ $Ca_v2.2$ channel recovery from block by R10K analogues was strongly determined by the HP. However, recovery of $Ca_v2.2$ channels in the presence of non-inactivating β_{2a} subunits was HP-independent. At a HP of –80 mV, $\alpha_{1B\text{-}b}/\alpha_2\delta_1/\beta_{2a}$ channels with profoundly slow inactivation completely recovered, whereas recovery of $\alpha_{1B\text{-}b}/\alpha_2\delta_1/\beta_3$ channels with fast inactivation was weak (Figure 3A,B). Previous experiments demonstrated that

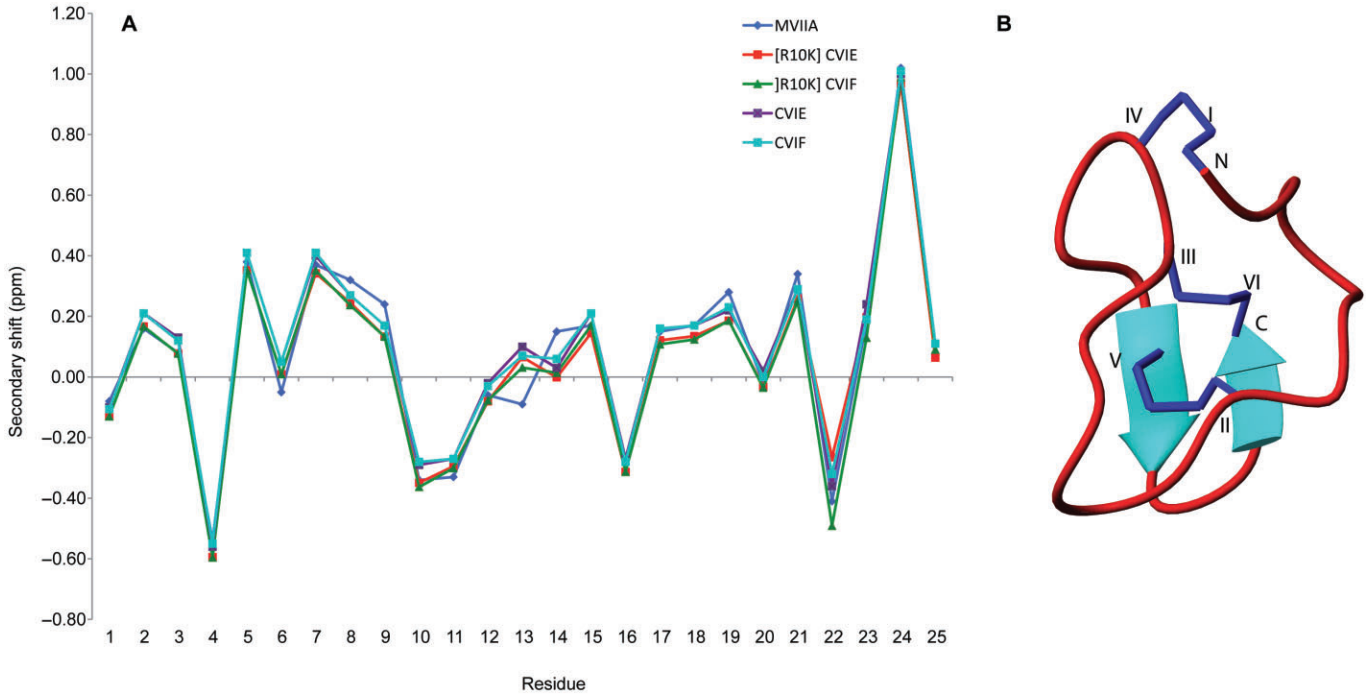

Figure 1

Comparison of the structures of various ω-conopeptides. (A) Hα secondary shifts for R10K-substituted ω-conopeptides CVIE&F compared with CVIE/CVIF and MVIIA. Secondary shifts were calculated by subtracting the random coil shifts (Wishart *et al.*, 1995) from the Hα chemical shifts. The chemical shifts for MVIIA were published by Atkinson *et al.* (2000). (B) Three-dimensional structure of MVIIA with the backbone shown in ribbon format (red), β-strands shown as arrows and disulfide bonds shown in stick format (blue) (PDB code 1TTK). This diagram was made using MOLMOL (Koradi *et al.*, 1996).

Table 2

Best-fit parameters for CVIE&F and [R10K]CVIE&F inhibition of VGCCs heterologously expressed in *Xenopus* oocytes and rat isolated DRG neurons

Cell type	VGCC	Peptide	IC_{50} (nM)	Hill slope	*n*	Reference
Xenopus oocyte	$\alpha_{1B\text{-}b} + \beta_3$	CVIE	0.12 ± 0.05	0.36 ± 0.04	6	Berecki *et al.* (2010)
		CVIF	0.10 ± 0.07	0.26 ± 0.04	7	Berecki *et al.* (2010)
	$\alpha_{1B\text{-}b} + \alpha_2\delta_1 + \beta_3$	CVIE	2.6 ± 0.5	0.45 ± 0.03	14	Berecki *et al.* (2010)
		CVIF	19.9 ± 3.2	0.51 ± 0.04	16	Berecki *et al.* (2010)
		[R10K]CVIE	[NS]3.5 ± 0.3	[a]0.57 ± 0.02	8	This study
		[R10K]CVIF	[b]7.6 ± 0.9	[c]0.65 ± 0.04	8	This study
	$\alpha_{1B\text{-}b} + \alpha_2\delta_1 + \beta_{2a}$	[R10K]CVIE	3.6 ± 0.3	0.84 ± 0.05	6	This study
		[R10K]CVIF	12.8 ± 0.8	0.86 ± 0.04	6	This study
DRG neuron	N-type	CVIE	11.1 ± 3.5	0.51 ± 0.05	6	This study
		CVIF	34.3 ± 2.1	0.42 ± 0.08	6	This study
		[R10K]CVIE	[NS]1.9 ± 3.6	[NS]0.64 ± 0.06	7	This study
		[R10K]CVIF	[d]2.2 ± 1.1	[NS]0.72 ± 0.16	7	This study

Values are determined by fitting concentration–response data to the Hill equation (see Methods section) and represented as mean ± SEM (*n*, number of oocytes). Significance of difference ($P < 0.05$) between CVIE and [R10K]CVIE or CVIF and [R10K]CVIF, at identical VGCC subunit compositions, was evaluated by Student's *t*-test.

[a]$P = 0.011$ versus CVIE, in oocytes expressing $\alpha_{1B\text{-}b} + \alpha_2\delta_1 + \beta_3$ subunits.

[b]$P = 0.014$ versus CVIF, in oocytes expressing $\alpha_{1B\text{-}b} + \alpha_2\delta_1 + \beta_3$ subunits.

[c]$P = 0.038$ versus CVIF in oocytes expressing $\alpha_{1B\text{-}b} + \alpha_2\delta_1 + \beta_3$ subunits.

[d]$P < 0.001$ versus CVIF, in DRG neurons.

NS, not significantly different from control.

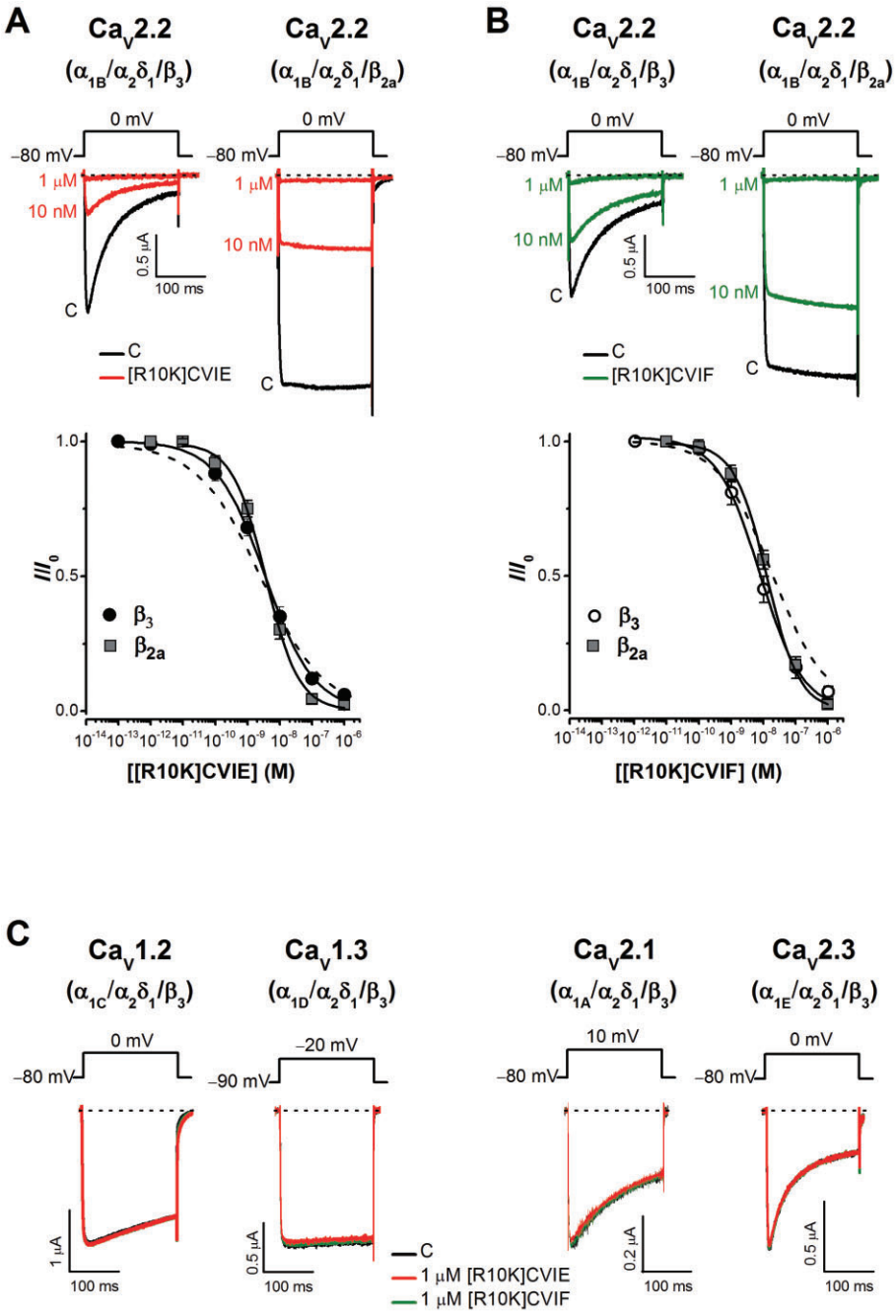

Figure 2

ω-Conopeptides [R10K]CVIE&F selectively block recombinant Ca$_v$2.2 channels in *Xenopus* oocytes. *Top*: Representative superimposed I_{Ba} obtained in the absence (C, control) and presence of 10 nM and 1 μM [R10K]CVIE (A) or [R10K]CVIF (B), from oocytes expressing fast-inactivating Ca$_v$2.2 ($\alpha_{1B\text{-}b}/\alpha_2\delta_1/\beta_3$) or slow-inactivating Ca$_v$2.2 ($\alpha_{1B\text{-}b}/\alpha_2\delta_1/\beta_{2a}$) VGCCs. I_{Ba} traces were evoked by 200 ms, 0.1 Hz step depolarizations to 0 mV from a HP of −80 mV (insets). Dotted lines indicate zero current level. Vertical bars represent 0.5 μA; horizontal bars represent 100 ms. *Bottom*: Cumulative concentration–response curves for [R10K]CVIE (A) or [R10K]CVIF (B) inhibition of $_{1B\text{-}b}/\alpha_2\delta_1/\beta_3$ or $\alpha_{1B\text{-}b}/\alpha_2\delta_1/\beta_{2a}$ VGCCs. Solid curves represent the best fit with the Hill equation (see Table 2 for IC_{50} and Hill coefficient values). Dashed lines represent fits with the Hill equation obtained for CVIE (A) or CVIF (B) block of N-type ($\alpha_{1B\text{-}b}/\alpha_2\delta1/\beta_3$) channels (Berecki *et al.*, 2010). (C) Representative superimposed I_{Ba} obtained in the absence (C, control) and presence of [R10K]CVIE (1 μM), followed by [R10K]CVIF (1 μM) after an ~2 min wash with external bath solution. Currents were evoked by 200 ms step depolarizations to 0 mV from a HP of −80 mV (Ca$_v$1.2 and Ca$_v$2.3); −20 mV from a HP of −90 mV (Ca$_v$1.3); or 10 mV from a HP of −80 mV (Ca$_v$2.1). Dotted line indicates zero current levels. *Top insets*: Voltage protocols.

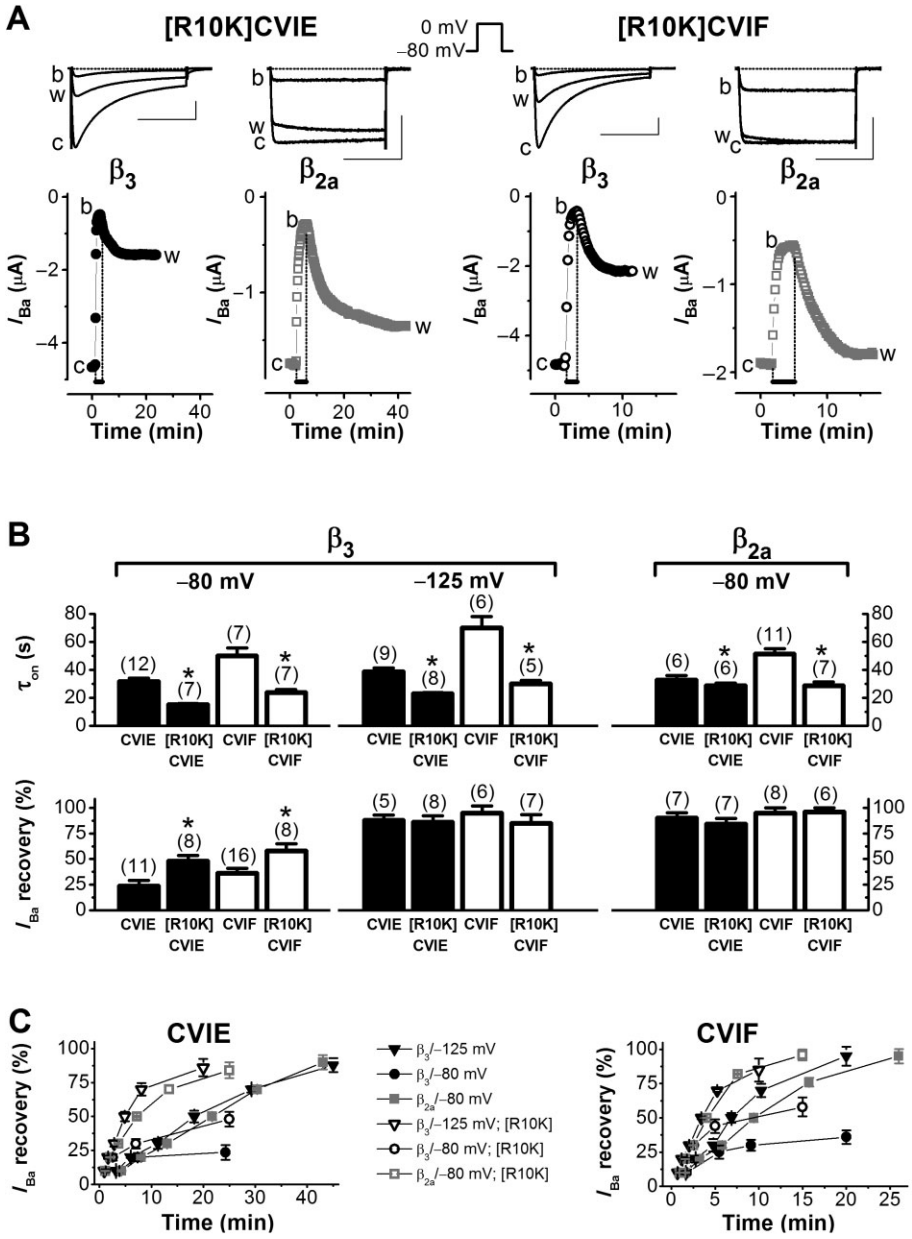

Figure 3

Time courses of [R10K]CVIE&F block display faster kinetics and better reversibility than those of CVIE&F in *Xenopus* oocytes. (A) β_3 and β_{2a} subunits largely affect reversibility at a close-to-physiological HP. Recombinant $Ca_v2.2$ channels with β_{2a} subunits almost completely recover from [R10K]CVIE or [R10K]CVIF block, whereas those with β_3 exhibit weaker recovery. *Top*: Representative superimposed traces of I_{Ba} evoked by 200 ms, 0.1 Hz depolarizations to 0 mV from a HP of –80 mV (*inset protocol*) in the absence (c, control; w, wash) and presence of 100 nM [R10K]CVIE or [R10K]CVIF (b, block). Bars represent 1 μA and 100 ms. Horizontal dotted lines indicate zero current level. *Bottom*: peak I_{Ba} values plotted as a function of time. Horizontal bars indicate the duration of ω-conopeptide application. (B) *Top*: Time constants of block by CVIE&F and their R10K analogues in oocytes expressing recombinant $Ca_v2.2$ channels with β_3 or β_{2a} subunits. Numbers in parentheses indicate the number of experiments. Asterisks (*) denote significant differences resulting from pairwise comparison of [R10K]CVIE with CVIE or [R10K]CVIF with CVIF at identical conditions (in all cases $^*P < 0.01$, Student's *t*-test). *Bottom*: Reversibility of block by 100 nM of ω-conotoxin CVIE or CVIF and their R10K analogues, as seen with $\alpha_{1B\text{-}b}/\alpha_2\delta_1/\beta_{2a}$ or $\alpha_{1B\text{-}b}/\alpha_2\delta_1/\beta_3$ VGCCs. Similar experimental voltage protocol as shown in (A). In a number of experiments, the HP was –125 mV. Asterisks (*) denote statistical differences resulting from pairwise comparison of [R10K]CVIE with CVIE or [R10K]CVIF with CVIF at –80 mV ($^*P < 0.05$, Student's *t*-test). C, Time course of VGCC ($\alpha_{1B\text{-}b}/\alpha_2\delta_1/\beta_{2a}$ or $\alpha_{1B\text{-}b}/\alpha_2\delta_1/\beta_3$) recovery from block by CVIE&F and their R10K analogues. Note the effect of hyperpolarization (–125 mV) on the magnitude and kinetics of I_{Ba} recovery compared with that at –80 mV. For each data point, $n \geq 5$ (see Table 3 for τ_{on} and τ_{off} values and extent of block and recovery).

Table 3

HP-dependent kinetics and extent of block and recovery from block by ω-conotoxins CVIE&F and [R10K]CVIE&F in *Xenopus* oocytes expressing $\alpha_{1B\text{-}b}/\beta_3$ or $\alpha_{1B\text{-}b}/\alpha_2\delta_1/\beta_3$ subunits

Subunits	Conotoxin (100 nM)	HP (mV)	τ_{off} (s)	k_{off} (s^{-1}x 10^{-3})	τ_{on} (s)	k_{on} ($M^{-1}\cdot s^{-1}$x10^5)	K_D[a] (nM)	I_{Ba} block (%)	I_{Ba} recovery (%)	*n*
$\alpha_{1B\text{-}b}+\beta_3$	CVIE	–80	541 ± 44	1.8 ± 0.1	10.4 ± 0.9	9.6 ± 0.7	1.9	93.4 ± 2.7	*34.1 ± 10	3–4
		–125	544 ± 11	1.8 ± 0.1	10.5 ± 1.2	9.5 ± 1.0	1.9	89.3 ± 5.0	100 ± 1.4	5–9
	CVIF	–80	313 ± 19	3.2 ± 0.1	14.1 ± 1.5	7.0 ± 0.8	4.6	89.6 ± 3.4	32.0 ± 6.3	4
		–125	359 ± 67	2.8 ± 0.5	14.7 ± 2.2	6.8 ± 1.0	4.1	80.3 ± 5.4	100 ± 4.0	3–4
$\alpha_{1B\text{-}b}+\alpha_2\delta_1+\beta_3$	CVIE	–80	225 ± 43	4.4 ± 0.8	31.5 ± 2.4	3.1 ± 0.6	14.2	86.3 ± 2.8	23.6 ± 5.4	9–13
		–125	1270 ± 120	0.8 ± 0.1	38.5 ± 2.8	2.6 ± 0.1	3.0	81.1 ± 3.2	87.8 ± 5.1	7–9
	CVIF	–80	256 ± 24	3.9 ± 0.4	50.0 ± 5.5	2.0 ± 0.2	19.5	79.2 ± 1.8	36.0 ± 4.9	16
		–125	717 ± 70	1.4 ± 0.2	70.0 ± 8.1	1.4 ± 0.1	9.7	74.7 ± 3.8	95.0 ± 6.8	6–7
	[R10K]CVIE	–80	323 ± 27	3.1 ± 0.3	*15.2 ± 0.8	6.6 ± 0.5	4.6	92.4 ± 1.1	*48.0 ± 5.5	8
		–125	*320 ± 35	3.1 ± 0.3	*22.8 ± 0.8	4.3 ± 0.1	7.1	81.6 ± 4.6	86.0 ± 6.3	7–8
	[R10K]CVIF	–80	208 ± 18	4.8 ± 0.4	*23.7 ± 2.2	4.3 ± 0.9	11.3	87.9 ± 2.4	*58.3 ± 6.9	8
		–125	*296 ± 27	3.3 ± 0.3	*30.0 ± 2.3	3.3 ± 0.2	10.1	78.0 ± 2.1	85.2 ± 8.4	5

The K_D values and percentages of I_{Ba} block and recovery were determined as described in the Methods section. Data are mean ± SEM (*n*, number of oocytes). For each peptide, asterisks (*) denote $P < 0.05$ statistical difference between CVIE and [R10K]CVIE or CVIF and [R10K]CVIF at identical HP values using Student's *t*-test for two groups.

[a]Similar estimates of potency (IC_{50}) were obtained using cumulative concentration–response data (Table 2).

$\alpha_{1B\text{-}b}/\alpha_2\delta_1/\beta_3$ channel recovery from CVID block was not affected by HP (Mould *et al.*, 2004), but recovery from MVIIA block exhibited a relatively weak voltage dependency (Stocker *et al.*, 1997). Recombinant N-type VGCC recovery from block by CVID or MVIIA could not be improved by replacing β_3 with β_{2a} subunits (not shown). We also determined the percentage of I_{Ba} recovery from block by [R10K]CVIE&F and CVIE&F (Figure 3B,C). Remarkably, R10K substitution in CVIE&F significantly improved $\alpha_{1B\text{-}b}/\alpha_2\delta_1/\beta_3$ $Ca_v2.2$ channel recovery from block at –80 mV.

The kinetics of ω-conotoxin action was dramatically affected by R10K substitution, resulting in faster block onset and recovery than those of CVIE or CVIF. For example, with $\alpha_{1B\text{-}b}/\alpha_2\delta_1/\beta_3$ channels, the time constants of block (τ_{on}) by [R10K]CVIE, 15.2 ± 0.8 (s) and 22.8 ± 0.8 (s), were almost twice as fast as those by CVIE, 31.5 ± 2.4 (s) and 38.5 ± 2.8 (s), at HPs of –80 or –125 mV respectively (Figure 3B and Table 3). For $_{1B\text{-}b}/\alpha_2\delta_1/\beta_3$ VGCCs, the washout times needed for 10, 20, 30, 50, 70 and ~90% recovery from [R10K]CVIE&F block were significantly (2–5 times) faster than washout times for CVIE&F at a HP of –125 (Figure 3C). Similar observations were made with $\alpha_{1B\text{-}b}/\alpha_2\delta_1/\beta_{2a}$ VGCCs at a HP of –80 mV (Figure 3C).

[R10K]CVIE&F inhibition of N-type VGCC in rat DRG neurons

[R10K]CVIE&F (1 nM–1 μM) potently reduced the peak I_{Ba} amplitude during step depolarizations to various membrane potentials from a HP of –80 mV, in small- and medium-sized DRG neurons (36.8 ± 2.8 pF; $n = 58$), classified according to Scroggs and Fox (1992). To determine which component of the whole-cell I_{Ba} was inhibited by these peptides, we examined the effect of [R10K]CVIE&F on low-voltage-activated T-type and high-voltage-activated (HVA) L-, N-, P/Q- and R-type currents, independently. We first elicited T-type currents by step depolarizations to –50 mV from a HP of –80 mV in small DRG neurons (26.7 ± 2.5 pF, $n = 10$). In these cells, [R10K]CVIE&F did not affect T-type currents ($n = 5$ for both peptides) (Figure 4A). HVA I_{Ba} was inhibited by [R10K]CVIE&F (1 μM) during step depolarizations to –5 mV or 0 mV from a HP of –80 mV. The residual I_{Ba} could be inhibited by subsequent applications of P/Q-type VGCC inhibitor ω-agatoxin-IVA (200 nM) and L-type VGCC inhibitor nifedipine (10 μM) ($n = 5$) (Figure 4B). Similar results were obtained with [R10K]CVIF (1 μM) ($n = 3$; data not shown). In four out of eight cells tested, the R-type VGCC blocker *SNX*-482 (100 nM) also inhibited a VGCC current component after [R10K]CVIE treatment (data not shown). These results indicate that [R10K]CVIE&F selectively blocks native N-type VGCCs in DRG neurons. Next, we applied increasing concentrations of CVIE&F or [R10K]CVIE&F to obtain concentration–response relationships described by Hill equations (Figure 4C–F). Also in DRG neurons, [R10K]CVIF resulted in a significantly higher inhibitory potency than that of CVIF (Table 2).

At a HP of –80 mV, we determined the percentage of inhibition and reversibility of inhibition by 100 nM ω-conotoxin CVIE or CVIF and their R10K analogues in DRG neurons. The percentage of N-type I_{Ba} fraction inhibited by CVIE&F or [R10K]CVIE&F was essentially the same (Figure 5A and Table 4). Similar to the results obtained with heterologously expressed $Ca_v2.2$ channels, R10K substitution significantly improved native N-type ($Ca_v2.2$) channel recovery from block at a HP of –80 mV ([R10K]CVIE&F) and –110 mV ([R10K]CVIE) (Figure 4G). At a HP of –80 mV, the onset time constants of N-type VGCCs inhibition were faster with

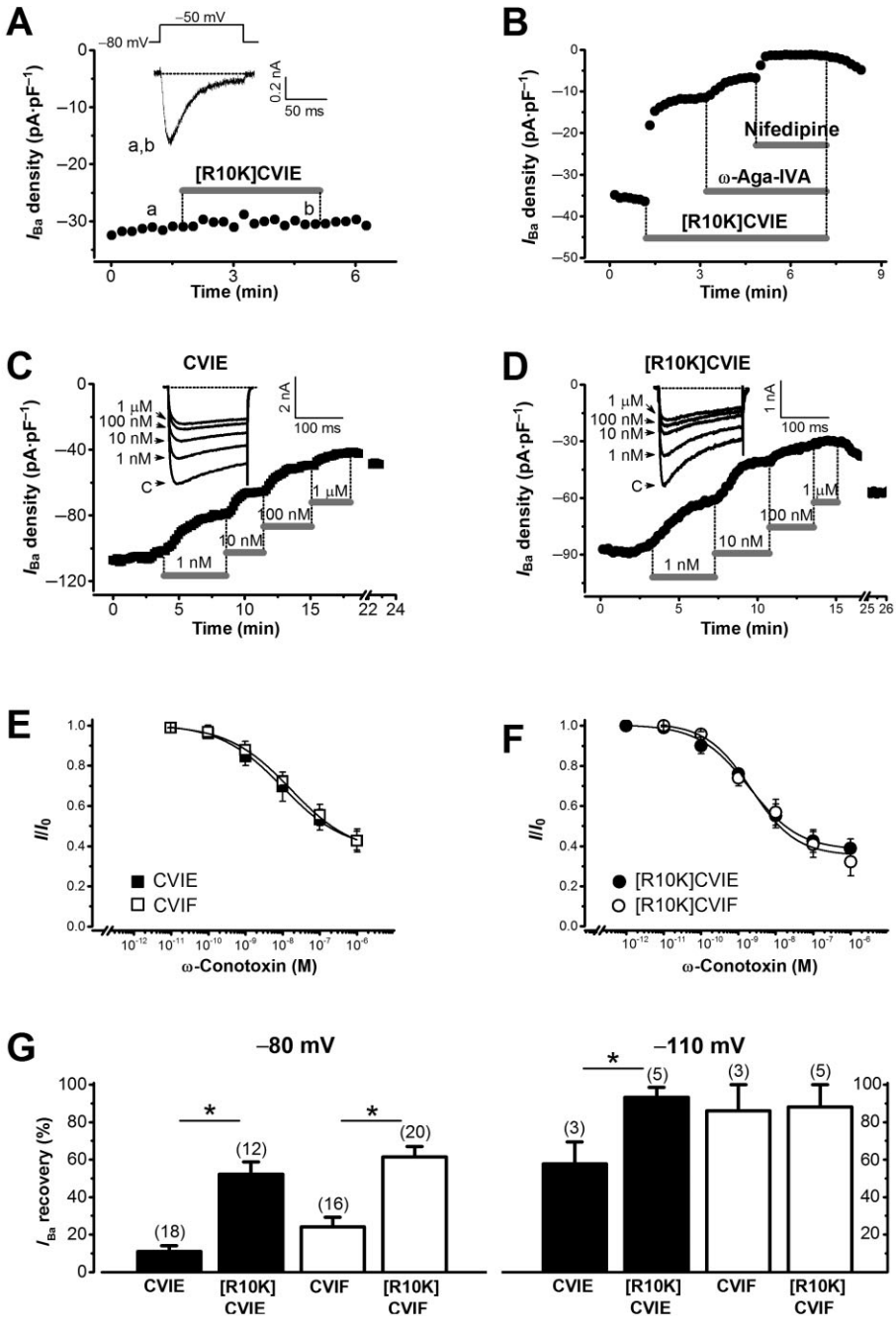

Figure 4

CVIE&F and [R10K]CVIE&F inhibition of I_{Ba} in rat DRG neurons. (A) [R10K]CVIE does not inhibit low-voltage-activated T-type VGCC currents. Time course of T-type current peak amplitude in the absence (a) and presence (b) of 1 μM [R10K]CVIE. I_{Ba} were elicited by 100 ms depolarizations to −50 mV from a HP of −80 mV, at frequencies of 1/15 or 1/10 s. *Inset*: Representative I_{Ba} traces at the times indicated by lower case letters. Horizontal dotted line indicates zero current level. (B) Time course of peak I_{Ba} inhibition by [R10K]CVIE and subsequent applications of ω-agatoxin-IVA (ω-Aga-IVA) and nifedipine (nif). The sequence and duration of drug application is indicated by horizontal bars. I_{Ba} were elicited from a HP of −80 mV by 150 ms depolarizations to 0 mV from a HP of −80 mV. (C) *Left*: Representative superimposed traces of I_{Ba} evoked by 80 ms, 0.1 Hz depolarizations to 0 mV from a HP of −80 mV in the absence (C, control) and presence of CVIE. The neuron was first exposed to control solution, then to increasing concentrations of CVIE. Dotted line indicates zero current level. *Right*: Time course of peak I_{Ba} during the onset of block in the presence of CVIE and after washout. Horizontal bars indicate the duration of CVIE application. (D) Similar experiment to that shown in (C) but using [R10K]CVIE instead of CVIE. (E, F) Cumulative concentration–response curves for normalized peak I_{Ba}. Solid curves represent the best fit with the Hill equation (see Table 2 for IC_{50} and Hill coefficient values). (G) Bar graph represents fractions of I_{Ba} recovery from block by 100 nM ω-conopeptide at HP values of −80 or −110 mV at the end of washout. Numbers in parentheses represent the number of DRG neurons. Asterisks (*) denote statistical differences resulting from pairwise comparison of [R10K]CVIE with CVIE or [R10K]CVIF with CVIF at HP −80 mV or HP −110 mV (*$P < 0.05$, Student's *t*-test).

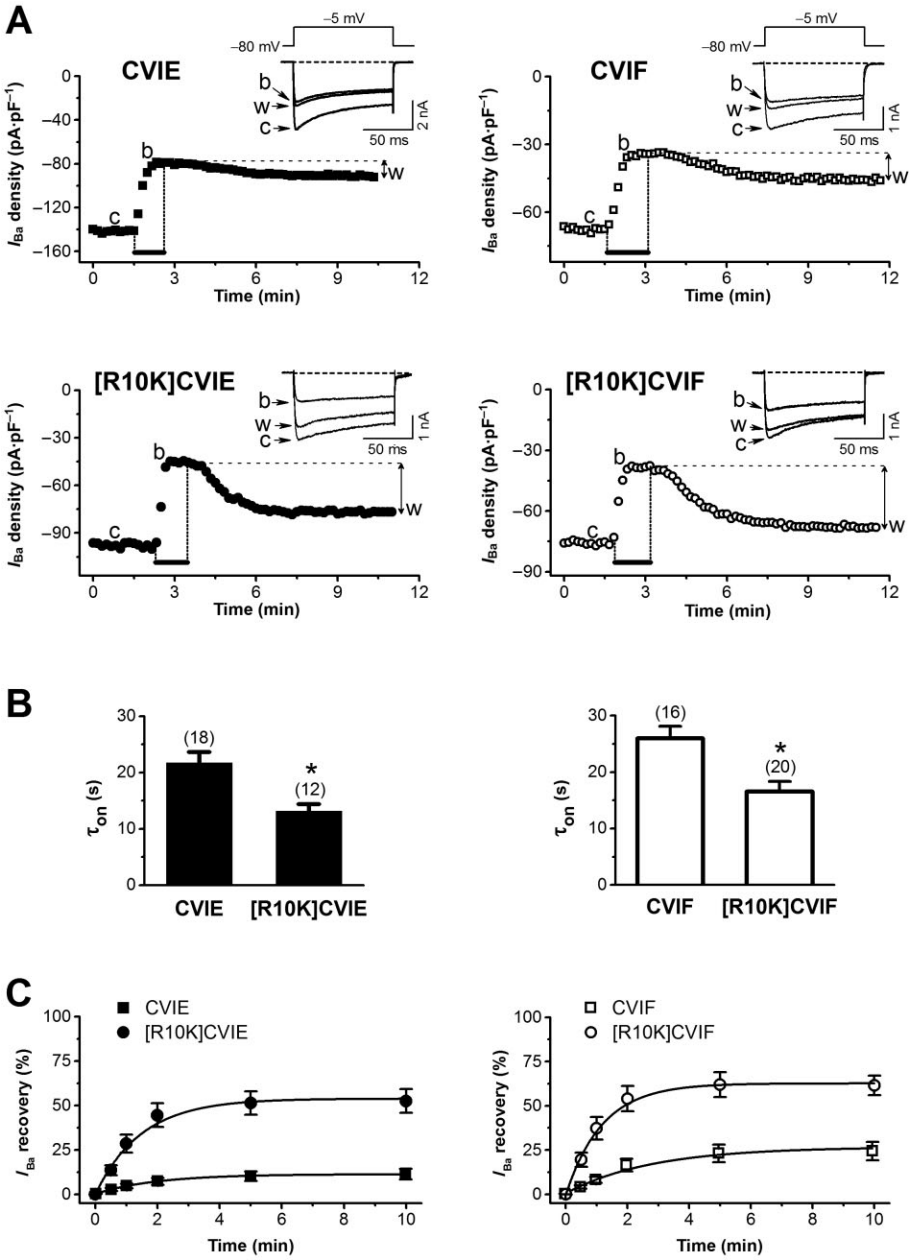

Figure 5

Kinetics of N-type VGCC inhibition and recovery by CVIE&F and their R10K analogues in DRG neurons. (A) [R10K]CVIE&F-inhibited N-type VGCCs exhibit greater reversibility compared with CVIE&F. Peak I_{Ba}, in the absence and presence of CVIE&F or [R10K]CVIE&F, was plotted as a function of time. Horizontal bars indicate the duration of peptide application. Insets show representative superimposed traces of I_{Ba} evoked by 100 ms, depolarizations (0.1 Hz) to −5 mV from a HP of −80 mV in the absence (c, control; w, wash) and presence of 100 nM [R10K]CVIE or [R10K]CVIF (b, block). (B) Time constants of inhibition (τ_{on}) at a HP of −80 mV, obtained by fitting peak I_{Ba} values shown in (A) during current inhibition to a mono-exponential function (see Methods section). Numbers in parentheses indicate the number of experiments. Asterisks (*) denote significant differences between [R10K]CVIE and CVIE (*P < 0.001, Student's t-test) or [R10K]CVIF and CVIF (*P < 0.003, Student's t-test). (C) Time course of N-type VGCC recovery from inhibition by CVIE&F and their R10K analogues at a HP of −80 mV. Recovery times were determined at various time points over 10 min washout. Offset time constants (τ_{off}) were obtained by fitting peak I_{Ba} values recorded during current recovery from inhibition to a mono-exponential function (see Methods section). See Table 4 for values of τ_{on}, τ_{off}, the percentage of inhibition and recovery and n (number of experiments). Note that τ_{off} values obtained for [R10K]CVIE&F did not reach statistical significance when compared with CVIE&F (P = 0.20 and 0.16 respectively).

Table 4

Kinetics of N-type VGCC inhibition, and extent of inhibition and recovery from inhibition, by ω-conotoxins CVIE&F and [R10K]CVIE&F at a HP of –80 mV in rat DRG neurons

Conotoxin (100 nM)	τ_{off} (s)	k_{off} ($s^{-1}x10^{-3}$)	τ_{on} (s)	k_{on} ($M^{-1}{\cdot}s^{-1}x10^{5}$)	K_D (nM)	I_{Ba} block (%)	I_{Ba} recovery (%)	*n*
CVIE	234 ± 54	4.2 ± 0.9	21.7 ± 1.9	4.6 ± 0.4	9.1	50.3 ± 3.5	11.1 ± 3.0	18
CVIF	169 ± 24	5.9 ± 0.8	26.0 ± 2.1	3.8 ± 0.3	15.5	52.1 ± 3.4	24.1 ± 5.2	12
[R10K]CVIE	142 ± 44	7.0 ± 2.1	*13.2 ± 1.2	7.5 ± 0.7	9.3	51.3 ± 2.4	*52.2 ± 6.6	16
[R10K]CVIF	125 ± 19	8.0 ± 1.2	*16.5 ± 1.8	6.1 ± 0.7	11.3	51.7 ± 3.8	*61.5 ± 5.6	20

The K_D values and percentages of I_{Ba} block and recovery were determined as described in the Methods section. Data are mean ± SEM (*n*, number of experiments). For each peptide, asterisks (*) denote statistical difference between CVIE and [R10K]CVIE or CVIF and [R10K]CVIF (see legends for Figures 4 and 5 for *P*-values).

[R10K]CVIE&F than CVIE&F, whereas the offset time constants remained similar (Figure 5 and Table 4). Altogether, these results indicate that R10K chemical modification significantly affected ω-conotoxin–N-type VGCC interaction.

Biological stability

The stability of the ω-conotoxins in human serum was evaluated to provide a guide as to their potential *in vivo* stability. The percentage of each ω-conotoxin remaining at various time points over 24 h in 100% human serum is shown in Figure 6. All of the tested ω-conotoxins were relatively stable, with approximately 20% of peptide remaining after 24 h incubation. In contrast, reduced forms of the peptides had completely degraded within 2 h. The observed decrease in peptide signals appears to be due to proteolytic degradation based upon fragmentation patterns observed using LC/MS (Applied Biosystems QSTAR Elite) and the observation that degradation of ω-conotoxin CVIE in serum was reduced significantly at 4°C (e.g. from 58.8 to 93.6% peptide remaining at the 6 h time point). Control samples in PBS solution showed that the binding of these conotoxins to serum proteins or polypropylene tubes was minimal (data not shown). The time-course studies indicate that [R10K] analogue stability is comparable with that of their parent peptides. CVIE&F was more stable than CVID ($P < 0.001$ at 6, 8, 12, and 24 h time points). Interestingly, ω-conotoxins are less stable than Vc1.1, a two-disulfide α-conotoxin that is exceptionally stable (Clark *et al.*, 2010), but their half-life in serum is still more than 6 h, which is significantly longer than the reduced peptides.

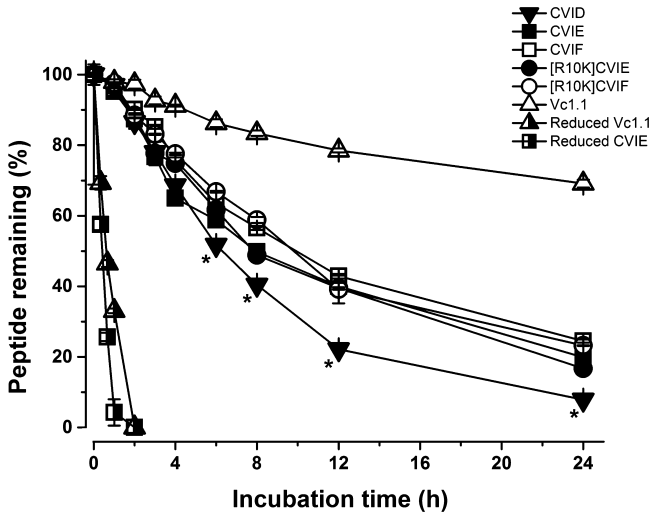

Figure 6

The stability of ω-conotoxins in human serum over 24 h. The peptide remaining in human serum after 24 h incubation was 7.9, 19.9, 24.5, 16.7, 23.2 and 69.1% for CVID, CVIE&F, [R10K]CVIE&F and Vc1.1 respectively. The serum stability of reduced forms of Vc1.1 and CVIE was included for comparison with the native peptides. The stability of reduced CVIF was similar to that of reduced CVIE (data not shown). Each data point represents the average of triplicates. Note that in many cases, the error bars are smaller than the data point symbols. Asterisks (*) denote that stability for CVID is significantly less than that of CVIE&F and [R10K]CVIE&F ($P < 0.001$, one-way ANOVA).

Discussion and conclusions

VGCCs are involved in various cellular functions, including neurotransmitter release, dendritic Ca^{2+} transient modulation and hormone release (Catterall *et al.*, 2005; Catterall, 2011). Among these, $Ca_v2.2$ channels are well-established pain signal mediators and validated targets for treating severe chronic pain (Williams *et al.*, 2008; Zamponi *et al.*, 2009).

Regulatory authorities in the USA and Europe have approved the use of ω-conotoxin MVIIA, with the generic name ziconotide and trade name Prialt (Miljanich, 2004), as an intrathecal analgesic for severe chronic pain. However, its use is often associated with adverse effects and it has a relatively narrow therapeutic window. Considerable effort has been devoted to engineering chemical modifications to conotoxins to improve their activity and stability (Craik and Adams, 2007) to overcome these problems.

The recently discovered ω-conotoxins CVIE&F potently and selectively inhibit recombinant $Ca_v2.2$ VGCCs expressed in *Xenopus* oocytes and native N-type VGCCs in rat DRG neurons (Berecki *et al.*, 2010). These compounds state-dependently interact with their ion channel target, exhibit-

ing higher affinity for inactivated $Ca_v2.2$ channels. This interaction can efficiently be disrupted by a hyperpolarizing HP, resulting in an efficient recovery from channel block. The auxiliary β and $\alpha_2\delta_1$ subunits also modulate ω-conotoxin binding to $Ca_v2.2$ channels. For example, the $\alpha_2\delta_1$ subunit reduces ω-conotoxin affinity for recombinant $Ca_v2.2$ channels (Mould *et al.*, 2004), the β_3 subunit conveys a relatively weak recovery from ω-conotoxin block, and $Ca_v2.2$ channels, including the non-inactivating β_{2a} subunit, almost completely recover from ω-conotoxin block (Berecki *et al.*, 2010).

It has been suggested that ω-conopeptide residue 10 has an important role in the extent of block reversibility, as shown by heterologously expressed $Ca_v2.2$ ($\alpha_{1B\text{-}b}/\alpha_2\delta_1/\beta_3$) channels recovering better from block by [R10K]MVIIA than MVIIA or [O10K]GVIA than block by GVIA (Mould *et al.*, 2004). However, in CVID, substituting lysine for arginine at position 10 ([K10R]CVID) impairs $\alpha_{1B\text{-}b}$ subunit recovery from block by [K10R]CVID when these subunits are expressed alone or co-expressed with β_3 subunits. However, it does not affect $\alpha_{1B\text{-}b}/\alpha_2\delta_1/\beta_3$ (peripheral N-type) VGCC recovery from block by [K10R]CVID. Somewhat surprisingly, $\alpha_{1B\text{-}d}/\alpha_2\delta_1/\beta_3$ (central N-type) VGCCs more efficiently recover from block by [K10R]CVID than from block by CVID (Mould *et al.*, 2004). This suggests that other amino acid residues may also influence the recovery process.

We designed the R10K substitution in CVIE&F and investigated their effects on conopeptide stability and $Ca_v2.2$ channel block. These substitutions dramatically quickened the blocking kinetics and significantly improved $Ca_v2.2$ channel recovery from block by these analogues (Tables 2 and 3), without loss of selectivity for $Ca_v2.2$. Usually, CVIE&F block of $Ca_v2.2$ channels is only weakly reversible. However, at –80 mV, $\alpha_{1B\text{-}b}/\alpha_2\delta_1/\beta_3$ $Ca_v2.2$ channels in *Xenopus* oocytes recovered significantly better from block by [R10K]CVIE&F than from block by CVIE&F. The faster onset times and improved $Ca_v2.2$ channel recovery from block by [R10K]CVIE/F *in vivo* may be better than other longer lasting N-type VGCC blockers such as CVID because they allow faster dose adjustment.

Interestingly, R10K substitution also resulted in increased CVIF potency. However, it should be noted that the mean estimates of IC_{50} and K_D values, determined from the concentration–response curves (Figure 2 and Table 2) and deduced from the time course of VGCC block and recovery (Table 3), respectively, were slightly different. This discrepancy could be attributed to variations in the estimates of K_D, which is more affected by errors in individual data points than IC_{50} (Barlow *et al.*, 1997). It should also be noted that the onset of inhibition of VGCCs by CVIE&F and [R10K]CVIE&F was concentration dependent and was only partially reversible. Therefore, it should be regarded as non-equilibrium, steady-state measurement (Christopoulos and Kenakin, 2002). Faster on-rates of block would yield Hill coefficients that are closer to one because the measurement conditions approach steady state (see Tables 2 and 3).

$Ca_v2.2$ channels exist in at least three distinct conformational states (closed, open and inactivated). We have shown that $Ca_v2.2$ channel inactivation determines the magnitude of I_{Ba} recovery from CVIE&F (Berecki *et al.*, 2010) and [R10K]CVIE&F block (Figure 3). The R10K substitution results in faster onset of block than those of CVIE&F at a HP of –80 mV. Regarding the process of recovery from block, it is plausible that conotoxin binding triggers a conformational change in the inactivated state that effectively locks the toxin to the binding site and controls the release of toxin from the channel. [R10K]CVIE&F peptides may be less efficient at inducing this conformational change compared with CVIE&F, resulting in more I_{Ba} recovery without a change in the offset time constants. Clearly, the R10K substitution is changing recovery, and as a result, more conotoxins are being washed out, but our data do not support increased off-rate as the mechanism.

The auxiliary β_3 subunit is prominently expressed in mammalian DRG neurons. It has been demonstrated that spinal nerve ligation significantly increases β_3 expression in these cells (Li *et al.*, 2012), highlighting the important role of this subunit in neuropathic pain. Our data show that N-type VGCCs recovered better from block by [R10K]CVIE&F in DRG neurons and the selectivity of the modified conotoxins for the N-type VGCC remained unchanged. Similar to results obtained with heterologously expressed $Ca_v2.2$ channels, the onset and recovery from block with [R10K]CVIE&F were faster than those of CVIE&F in DRG neurons.

NMR spectroscopy studies did not reveal any significant change in the conserved ω-conotoxin backbone conformation after R10K substitution. Since the three-dimensional peptide fold did not change, the altered kinetic properties could be either due to the introduced lysine in CVIE&F changing the binding configuration of these ω-conopeptides in the pore vestibule region of the $Ca_v2.2$ channel, or modified local binding interactions associated with the substituted residue. Since both on- and off-rates were affected by the substitution, the former explanation appears more likely.

Only a limited amount of data is available on the bioavailability and stability of clinically used ziconotide in plasma or CSF (Newcomb *et al.*, 2000; Wermeling *et al.*, 2003; Yaksh *et al.*, 2012). In our study, the proteolytic stability of CVID, CVIE&F and their analogues was investigated in human serum since it incorporates a highly active mixture of proteases that provides a robust 'test' of peptide stability. Figure 6 shows that all the tested ω-conotoxins remain stable (i.e. >75% unchanged) in human serum for at least 4 h, with the median half-life more than 6 h. By contrast, the half-life of the reduced peptides is less than 40 min. This clearly indicates that the cystine knot motif plays an important role in the serum stability of these conotoxins. The time-course analysis of CVIE and CVIF showed similar trends in proteolytic degradation, whereas CVID was less stable. Given that CVID, CVIE and CVIF are similar in structure and all contain a cystine knot motif, the observed difference in stability must reflect their amino acid compositions. CVIE and CVIF have high sequence identity (>95%). By contrast, CVID is only 60% identical in sequence to CVIE and CVIF, and contains different residues at positions 3, 7, 9, 10, 11, 12, 17 and 21–24. Although these data provide insights into the ω-conotoxins stability to ubiquitous peptidases in human serum, it is not clear how the peptides would behave in CSF since the peptidase composition in CSF is different from plasma and the proteolytic activity is highly sequence dependent. Moreover, another mechanism can theoretically be accountable for drug lifetimes in CSF. Pharmacokinetic studies of ziconotide (MVIIA) in chronic pain patients suggest

that the main pathway for ziconotide clearance is the bulk redistribution of CSF (Wermeling *et al.*, 2003). A later study using a canine model came to a similar conclusion for ziconotide clearance (Yaksh *et al.*, 2012). Since bulk CSF flow significantly determines the removal of ziconotide in CSF, the metabolism of ω-conotoxins in CSF would be primarily dependent upon the CSF flow rate.

Interestingly, the wild-type and mutant ω-conotoxins are less stable than Vc1.1, a two-disulfide α-conotoxin that inhibits $Ca_v2.2$ channels through $GABA_B$ receptor-mediated pathways (Callaghan *et al.*, 2008; Cuny *et al.*, 2012), and is reported to be exceptionally stable (Clark *et al.*, 2010). However, it could be argued that a relatively short biological half-life is beneficial for ω-conotoxins that maintain a narrow therapeutic window because it enables relatively rapid plasma clearance and/or reduces adverse effects after administration.

It is increasingly evident that kinetic data on drug–protein interactions can help generate compounds with optimized kinetic profiles for target binding (Andersson *et al.*, 2006). Clinical efficacy, duration of action, clinical differentiation and safety may all be influenced by binding kinetics (Swinney, 2009). CVID has a wider therapeutic window than MVIIA in rat models of inflammatory and neuropathic pain (Scott *et al.*, 2002), and it has been suggested that the differences in these conotoxins' biophysical and pharmacokinetic properties could explain this (Adams *et al.*, 2003; Mould *et al.*, 2004). However, in a preclinical model of neuropathic pain, intrathecally administered CVID reduced pain only marginally more than MVIIA did, and this did not appear to be related to reversibility of $Ca_v2.2$ channel block (Jayamanne *et al.*, 2013).

Systemically administered CVID and CVIE reversed signs of inflammatory pain without neurological side effects, such as motor deficits or sedation, in a mouse chronic inflammatory pain model (Sadeghi *et al.*, 2013a). Preliminary data suggest that systemically administered [R10K]CVIE&F also reduce inflammatory pain with efficacy similar to CVIE, and without noticeable side effects, in a complete Freund's adjuvant-induced inflammatory mouse pain model (Sadeghi *et al.*, 2013b). Despite R10K mutations apparently having little effect on CVID- or MVIIA-induced analgesia (Jayamanne *et al.*, 2013), it is useful to establish whether [R10K]CVIE&F's faster kinetics and improved reversibility results in a better analgesic window and fewer side effects than previously characterized $Ca_v2.2$ blockers. The ability to modulate on- and off-rates could be particularly valuable to adjust sub-optimal pharmacokinetics *in vivo*, with a high on-rate possibly decreasing the time a peptide needs to interact with the binding site.

In summary, R10K substitution in CVIE&F significantly changes the kinetics of ω-conotoxin action and improves reversibility, without diminishing conotoxin potency or specificity for VGCCs. However, further studies are needed to clarify the full therapeutic potential of these compounds.

Acknowledgements

This work was supported by a National Health and Medical Research Council (NHMRC) Program Grant (P. F. A. and D. J. A.), NHMRC Project Grant 1034642 (G. B.) and a University of Queensland Postdoctoral Research Fellowship (G.B.). D. J. C. is an NHMRC Senior Principal Research Fellow and D. J. A. is an Australian Research Council (ARC) Australian Professorial Fellow. N. L. D. was supported by a Queensland Smart State Fellowship and is an ARC Future Fellow.

Conflict of interest

G. B., P. F. A. and D. J. A. have filed a provisional patent related to this manuscript: Novel ω-conotoxin peptides; 2010 National Phase PCT/AU2010/001228. The authors declare no other competing interests.

References

Adams DJ, Smith AB, Schroeder CI, Yasuda T, Lewis RJ (2003). ω-Conotoxin CVID inhibits a pharmacologically distinct voltage-sensitive calcium channel associated with transmitter release from preganglionic nerve terminals. J Biol Chem 278: 4057–4062.

Adams DJ, Callaghan B, Berecki G (2012). Analgesic conotoxins: block and G protein-coupled receptor modulation of N-type $Ca_V2.2$ calcium channels. Br J Pharmacol 166: 486–500.

Alexander SPH, Benson HE, Faccenda E, Pawson AJ, Sharman JL, Spedding M, Peters JA, Harmar AJ and CGTP Collaborators (2013). The Concise Guide to PHARMACOLOGY 2013/14: Ion channels. Br J Pharmacol 170: 1607–1651.

Altier C, Zamponi GW (2004). Targeting Ca^{2+} channels to treat pain: T-type versus N-type. Trends Pharmacol Sci 25: 465–470.

Andersson K, Karlsson R, Lofas S, Franklin G, Hamalainen MD (2006). Label-free kinetic binding data as a decisive element in drug discovery. Expert Opin Drug Discov 1: 439–446.

Atkinson RA, Kieffer B, Dejaegere A, Sirockin F, Lefevre JF (2000). Structural and dynamic characterization of ω-conotoxin MVIIA: the binding loop exhibits slow conformational exchange. Biochemistry 39: 3908–3919.

Barlow RB, Bond SM, Bream E, Macfarlane L, McQueen DS (1997). Antagonist inhibition curves and the measurement of dissociation constants. Br J Pharmacol 120: 13–18.

Berecki G, Motin L, Haythornthwaite A, Vink S, Bansal P, Drinkwater R *et al.* (2010). Analgesic ω-conotoxins CVIE and CVIF selectively and voltage-dependently block recombinant and native N-type calcium channels. Mol Pharmacol 77: 139–148.

Bingham JP, Mitsunaga E, Bergeron ZL (2010). Drugs from slugs – past, present and future perspectives of ω-conotoxin research. Chem Biol Interact 183: 1–18.

Bulaj G, Olivera BM (2008). Folding of conotoxins: formation of the native disulfide bridges during chemical synthesis and biosynthesis of *Conus* peptides. Antioxid Redox Signal 10: 141–155.

Callaghan B, Haythornthwaite A, Berecki G, Clark RJ, Craik DJ, Adams DJ (2008). Analgesic α-conotoxins Vc1.1 and Rg1A inhibit N-type calcium channels in rat sensory neurons via $GABA_B$ receptor activation. J Neurosci 28: 10943–10951.

Catterall WA (2011). Voltage-gated calcium channels. Cold Spring Harb Perspect Biol 3: a003947.

Catterall WA, Perez-Reyes E, Snutch TP, Striessnig J (2005). International Union of Pharmacology. XLVIII. Nomenclature and structure-function relationships of voltage-gated calcium channels. Pharmacol Rev 57: 411–425.

Christopoulos A, Kenakin T (2002). G protein-coupled receptor allosterism and complexing. Pharmacol Rev 54: 323–374.

Clark RJ, Jensen J, Nevin ST, Callaghan BP, Adams DJ, Craik DJ (2010). The engineering of an orally active conotoxin for the treatment of neuropathic pain. Angew Chem Int Ed Engl 49: 6545–6548.

Craik DJ, Adams DJ (2007). Chemical modification of conotoxins to improve stability and activity. ACS Chem Biol 2: 457–468.

Craik DJ, Daly NL, Waine C (2001). The cystine knot motif in toxins and implications for drug design. Toxicon 39: 43–60.

Cuny H, de Faoite A, Huynh T, Yasuda T, Berecki G, Adams DJ (2012). γ-Aminobutyric acid type B ($GABA_B$) receptor expression needed for inhibition of N-type ($Ca_v2.2$) calcium channels by analgesic α-conotoxins. J Biol Chem 287: 23948–23957.

Hatakeyama S, Wakamori M, Ino M, Miyamoto N, Takahashi E, Yoshinaga T *et al*. (2001). Differential nociceptive responses in mice lacking the α_{1B} subunit of N-type Ca^{2+} channels. Neuroreport 12: 2423–2427.

Jaggi AS, Jain V, Singh N (2011). Animal models of neuropathic pain. Fundam Clin Pharmacol 25: 1–28.

Jayamanne A, Jeong HJ, Schroeder CI, Lewis RJ, Christie MJ, Vaughan CW (2013). Spinal actions of ω-conotoxins, CVID, MVIIA and related peptides in a rat neuropathic pain model. Br J Pharmacol 170: 245–254.

Kilkenny C, Browne W, Cuthill IC, Emerson M, Altman DG (2010). Animal research: reporting in vivo experiments: the ARRIVE guidelines. Br J Pharmacol 160: 1577–1579.

Kim JI, Takahashi M, Ogura A, Kohno T, Kudo Y, Sato K (1994). Hydroxyl group of Tyr^{13} is essential for the activity of ω-conotoxin GVIA, a peptide toxin for N-type calcium channel. J Biol Chem 269: 23876–23878.

Koradi R, Billeter M, Wuthrich K (1996). MOLMOL: a program for display and analysis of macromolecular structures. J Mol Graph 14: 51–55, 29–32.

Lewis RJ, Nielsen KJ, Craik DJ, Loughnan ML, Adams DA, Sharpe IA *et al*. (2000). Novel ω-conotoxins from *Conus catus* discriminate among neuronal calcium channel subtypes. J Biol Chem 275: 35335–35344.

Lewis RJ, Dutertre S, Vetter I, Christie MJ (2012). *Conus* venom peptide pharmacology. Pharmacol Rev 64: 259–298.

Li L, Cao XH, Chen SR, Han HD, Lopez-Berestein G, Sood AK *et al*. (2012). Up-regulation of $Ca_v\beta_3$ subunit in primary sensory neurons increases voltage-activated Ca^{2+} channel activity and nociceptive input in neuropathic pain. J Biol Chem 287: 6002–6013.

McGivern JG (2006). Targeting N-type and T-type calcium channels for the treatment of pain. Drug Discov Today 11: 245–253.

McGrath JC, Drummond GB, McLachlan EM, Kilkenny C, Wainwright CL (2010). Guidelines for reporting experiments involving animals: the ARRIVE guidelines. Br J Pharmacol 160: 1573–1576.

Miljanich GP (2004). Ziconotide: neuronal calcium channel blocker for treating severe chronic pain. Curr Med Chem 11: 3029–3040.

Motin L, Yasuda T, Schroeder CI, Lewis RJ, Adams DJ (2007). ω-conotoxin CVIB differentially inhibits native and recombinant N- and P/Q-type calcium channels. Eur J Neurosci 25: 435–444.

Mould J, Yasuda T, Schroeder CI, Beedle AM, Doering CJ, Zamponi GW *et al*. (2004). The $\alpha_2\delta$ auxiliary subunit reduces affinity of ω-conotoxins for recombinant N-type ($Ca_v2.2$) calcium channels. J Biol Chem 279: 34705–34714.

Newcomb R, Abbruscato TJ, Singh T, Nadasdi L, Davis TP, Miljanich G (2000). Bioavailability of ziconotide in brain: influx from blood, stability, and diffusion. Peptides 21: 491–501.

Nielsen KJ, Adams DA, Alewood PF, Lewis RJ, Thomas L, Schroeder T *et al*. (1999). Effects of chirality at Tyr13 on the structure-activity relationships of ω-conotoxins from *Conus* magus. Biochemistry 38: 6741–6751.

Olivera BM, Miljanich GP, Ramachandran J, Adams ME (1994). Calcium channel diversity and neurotransmitter release: the ω-conotoxins and ω-agatoxins. Annu Rev Biochem 63: 823–867.

Sadeghi M, Murali SS, Lewis RJ, Alewood PF, Mohammadi S, Christie MJ (2013a). Novel ω-conotoxins from *Conus catus* reverse signs of mouse inflammatory pain after systemic administration. Mol Pain 9: 51.

Sadeghi M, Murali SS, Alewood PF, Christie MJ (2013b). Novel ω-conotoxins potently inhibit N-type voltage-gated calcium channels in sensory neurons and partially reverse pain behavior after systemic dosing. Proc Aust Neurosci Soc 23: 151. Abstract.

Schmidtko A, Lotsch J, Freynhagen R, Geisslinger G (2010). Ziconotide for treatment of severe chronic pain. Lancet 375: 1569–1577.

Schnölzer M, Alewood P, Jones A, Alewood D, Kent SB (1992). *In situ* neutralization in Boc-chemistry solid phase peptide synthesis. Rapid, high yield assembly of difficult sequences. Int J Pept Protein Res 40: 180–193.

Schroeder CI, Doering CJ, Zamponi GW, Lewis RJ (2006). N-type calcium channel blockers: novel therapeutics for the treatment of pain. Med Chem 2: 535–543.

Scott DA, Wright CE, Angus JA (2002). Actions of intrathecal ω-conotoxins CVID, GVIA, MVIIA, and morphine in acute and neuropathic pain in the rat. Eur J Pharmacol 451: 279–286.

Scroggs RS, Fox AP (1992). Calcium current variation between acutely isolated adult rat dorsal root ganglion neurons of different size. J Physiol 445: 639–658.

Snutch TP (2005). Targeting chronic and neuropathic pain: the N-type calcium channel comes of age. NeuroRx 2: 662–670.

Stocker JW, Nadasdi L, Aldrich RW, Tsien RW (1997). Preferential interaction of ω-conotoxins with inactivated N-type Ca^{2+} channels. J Neurosci 17: 3002–3013.

Swinney DC (2009). The role of binding kinetics in therapeutically useful drug action. Current Opin Drug Discov Devel 12: 31–39.

Terlau H, Olivera BM (2004). *Conus* venoms: a rich source of novel ion channel-targeted peptides. Physiol Rev 84: 41–68.

Vink S, Alewood P (2012). Targeting voltage-gated calcium channels: developments in peptide and small-molecule inhibitors for the treatment of neuropathic pain. Br J Pharmacol 167: 970–989.

Wallace MS, Rauck RL, Deer T (2010). Ziconotide combination intrathecal therapy: rationale and evidence. Clin J Pain 26: 635–644.

Wermeling D, Drass M, Ellis D, Mayo M, McGuire D, O'Connell D *et al*. (2003). Pharmacokinetics and pharmacodynamics of

intrathecal ziconotide in chronic pain patients. J Clin Pharmacol 43: 624–636.

Williams JA, Day M, Heavner JE (2008). Ziconotide: an update and review. Expert Opin Pharmacother 9: 1575–1583.

Wishart DS, Bigam CG, Holm A, Hodges RS, Sykes BD (1995). 1H, 13C and 15N random coil NMR chemical shifts of the common amino acids. I. Investigations of nearest-neighbor effects. J Biomol NMR 5: 67–81.

Yaksh TL, de Kater A, Dean R, Best BM, Miljanich GP (2012). Pharmacokinetic analysis of ziconotide (SNX-111), an intrathecal N-type calcium channel blocking analgesic, delivered by bolus and infusion in the dog. Neuromodulation 15: 508–519.

Zamponi GW, Lewis RJ, Todorovic SM, Arneric SP, Snutch TP (2009). Role of voltage-gated calcium channels in ascending pain pathways. Brain Res Rev 60: 84–89.